Thermal and fluidic characterization of Tesla valve via computational fluid dynamics

By

Piyush Porwal

A Thesis
Submitted to the Faculty of
Mississippi State University
in Partial Fulfillment of the Requirements
for the Degree of Master of Science
in Mechanical Engineering
in the Department of Mechanical Engineering

Mississippi State, Mississippi

May 2016

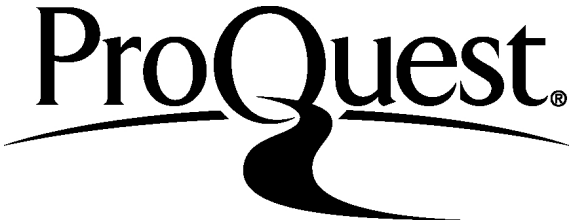

Thermal and fluidic characterization of Tesla valve via computational fluid dynamics

By

Piyush Porwal

Approved:

_____

Scott M. Thompson
(Major Professor)

_____

Pedro J. Mago
(Committee Member)

_____

D. Keith Walters
(Committee Member / Graduate Coordinator)

_____

Jason M.Keith
Dean
Bagley College of Engineering

Name: Piyush Porwal

Date of Degree: May 6, 2016

Institution: Mississippi State University

Major Field: Mechanical Engineering

Director of Thesis: Dr. Scott M. Thompson

Title of Study: Thermal and fluidic characterization of Tesla valve via computational fluid dynamics

Pages in Study 47

Candidate for Degree of Master of Science

Tesla valve applications for passive flow enhancement in micro fluidic applications are promising, because of its design of no-moving-parts. The effectiveness of the valve (measured via its pressure and thermal diodicity) can be increased by creating a multi-staged Tesla valve. Present study investigates the effect of varying Reynolds number (25-200) on flow rectification and thermal enhancement capability of a Tesla valve. Gamboa Morris Forster (GMF) design with a cross-section of $1mm^2$ and constant valve-to-valve distance (1mm) was utilized for this research. An arbitrary fluid with constant properties at a reference temperature was used as the working fluid. Periodicity in flow and thermal distribution are noticed in the latter part of MSTV. Average friction factor and pressure diodicity decreased with increasing Reynolds number whereas average Nusselt number and thermal diodicity increased. Correlations for friction factor, pressure diodicity, Nusselt number, and thermal diodicity were derived by fitting a non-linear curve fit model.

ACKNOWLEDGEMENTS

I would like to express my sincere thanks to Dr. Scott M. Thompson, under whose guidance and support I was able to accomplish my research goals. He has always been a driving force which compelled me achieve more. His hard working and tireless attitude always inspired to strive harder.

I am also very grateful to Dr. Keith Walters for his supervision and patience during my research work. He helped me develop analytical thinking and become a better researcher. I also appreciate Dr. Pedro Mago for his valuable insights and encouragement.

Most importantly, I give my deepest gratitude to my parents and friends without whom this journey would have been impossible. Their unconditional love and support gave me the strength to accomplish my goals.

Lastly, I would like to thank god for his blessings and grace which gave me the strength to keep going and achieve my goals.

TABLE OF CONTENTS

LIST OF TABLES

LIST OF FIGURES

NOMENCLATURE

A_c	cross-sectional area, m^2
C_p	isobaric specific heat capacity, J/kg·K
D	diameter, m
D_H	hydraulic diameter,m
Di_P	pressure diodicity
Di_T	thermal diodicity
E	total energy, J
f	friction factor
$\bar{f}$	average friction factor
$\bar{f}_{1,fwd}$	average friction factor for first valve (forward flow)
$\bar{f}_{\infty,fwd}$	average friction factor for tenth valve (forward flow)
$\bar{f}_{1,rev}$	average friction factor for first valve (reverse flow)
$\bar{f}_{\infty,rev}$	average friction factor for tenth valve (reverse flow)
G	*valve to valve distance*
H	height, m
$\bar{h}$	average heat transfer coefficient, $W/m^2 \cdot K$
k	thermal conductivity, W/m·K
$\dot{m}$	mass flow rate, kg/s
$\overline{Nu}$	average Nusselt number
N	number of Tesla valves (stages)
$\overline{Nu}_{1,fwd}$	average nusselt number for first valve (forward flow)
$\overline{Nu}_{\infty,fwd}$	average nusselt number for tenth valve (forward flow)
$\overline{Nu}_{1,rev}$	average nusselt number for first valve (reverse flow)
$\overline{Nu}_{\infty,rev}$	average nusselt number for tenth valve (reverse flow)

P	static pressure, Pa
Pr	Prandlt number
q	heat transfer rate, W/m^2
Re	Reynolds number
ΔT	temperature difference, K
ΔT_{LM}	log-mean temperature difference
u	velocity field, m/s
W	width, m

Greek symbols

δ	momentum boundary layer entrance length, m
μ	dynamic viscosity, Pa·s
v	kinematic viscosity, m^2/s
ρ	density, kg/m
τ_{eff}	effective viscous dissipation

Subscripts

i	inlet
w	wall
o	outlet
l,j	index

CHAPTER I

INTRODUCTION

Introduction of the concept of micro and mini sized channels by Tuckerman and Pease [1] in 1981 revolutionized the electronic industry. Through their experiments they proved that for laminar flows in confined channels, convective heat transfer coefficient (h) inversely favors channel width. While designing the heat sink, it was found that coolant viscosity governed the channel width. These results opened up a vast field of applications of micro and mini channels for flow control and thermal enhancement. Today micro channels have diversified applications. They are used in electronic & medical applications, microelectro-mechanical systems (MEMS), micro heat exchangers, pumps, mixers, sensor and actuators.

1.1 Classification of micro-channels

Micro-channels essentially differ from conventional channels in terms of the hydraulic diameter. Diameter of micro-channels is generally less than 1mm. Mehandale et al. came up with classification of channels based on the dimensions of the channel [2]. This classification is shown in table 1.1.

Table 1.1 Channels classification by Mehendale [2]

Channels	Hydraulic Diameter (D_H)
Conventional channel	$D_H > 6$ mm
Compact passage	1 mm $< D_H \leq 6$ mm
Meso channel	100 μm $< D_H \leq 1$ mm
Micro channel	1 μm $< D_H \leq 100$ μm

Kandlikar et al. proposed a refined classification of channels depending on the flow considerations (mainly Knudson number) and manufacturing considerations [3]. Table 1.2 details the Kandlikar classification of channels.

Table 1.2 Channels classification by Kandlikar [3]

Channels	Hydraulic Diameter (D_H)
Conventional channel	$D_H > 3$ mm
Mini channel	200 μm $< D_H \leq 3$ mm
Micro channel	10 μm $< D_H \leq 200$ μm
Transitional channel	0.1 μm $< D_H \leq 10$ μm
Molecular nano-channel	$D_H \leq 0.1$ μm

1.2 Methods for flow control and thermal enhancement in micro channels

Although high surface to volume ratio makes micro-channels an excellent measure for flow rectification and thermal enhancement, additional techniques are required to enhance the efficiency of micro channels. Steinke et al. and Kandlikar et al. reviewed single phase enhancement techniques for application in micro and mini channels [4]. They discussed two techniques namely active and passive. Active techniques need additional external source of power like electricity, RF signals or pumps. Use of actuators, micro pump, electrostatic fields and synthetic jets are popular active

flow control techniques. Passive flow control techniques does not involve use of any external power source. Some basic techniques are listed and discussed below.

- Flow disruption – Implementation of flow inserts and obstacles in the flow (in the form of check valves) causes enhanced mixing, flow transition and development of secondary flow.
- Secondary flow – Incorporation of offset strip fins, chevron plates and venturi are some methods that can be used to generate secondary flows to enhance fluid mixing.
- Surface treatments – Surface of channel can be treated to make it hydrophilic or hydrophobic to alter the flow field and control local liquid surface interaction.
- Entrance effects – A constant flow development causing enhanced mixing can be achieved by inclusion of entrance effects caused by sudden expansion and contraction in flow area of the micro channel.

1.3 Check valve

Check valves are passive flow control devices used for fluid rectification purposes. They are integrated in channels as moving parts in the form of flaps, spherical balls, heart shape, triangle etc. Check valves display a diode like behavior by allowing only forward flow in the channel, essential for fluid rectification. Flow in a single direction is obtained at the expense of minor pressure losses. Different check valve designs in practice are shown in Fig. 1.1.

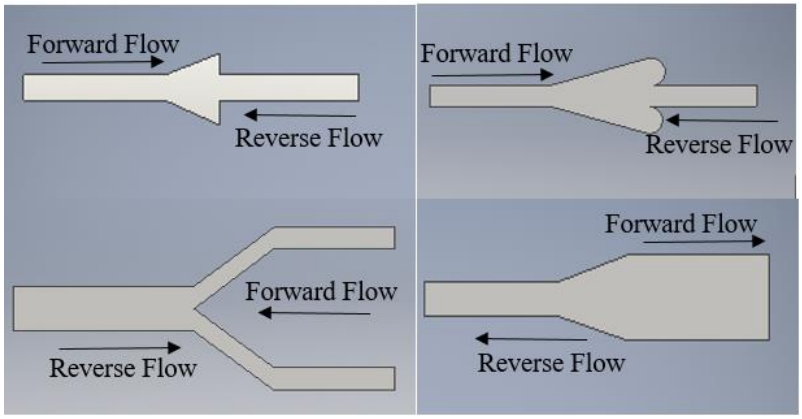

Figure 1.1 Check valve designs

1.4 Tesla valve

The valvular conduit, or Tesla valve, is a check valvefirst introduced in 1920 by Tesla [5]. Initially intended for gaseous flow control, the device consists of no moving parts and requires no external power for operation (i.e. is passive). The valve functions as a fluidic diode – allowing for preferential (or "forward") and "reverse" flow directions due to its unique design features providing for direction-dependent pressure drops (shown in Fig. 1.2). There are a variety of passive-type, no-moving-parts check valves for fluidic rectification and flow control, including the nozzle/diffuser valve [6], terminal check valve [7],bridge check valve [7], and ball shaped check valves[8]. Compared to other valves, the Tesla valve design is more geared toward flow control via bifurcation and jet impingement mechanisms. Typically, a Tesla valve possesses two flow paths, namely a helix part and a trunk part. Trunk part is the straight channel part whereas helix part is a curved part which restricts backflow.

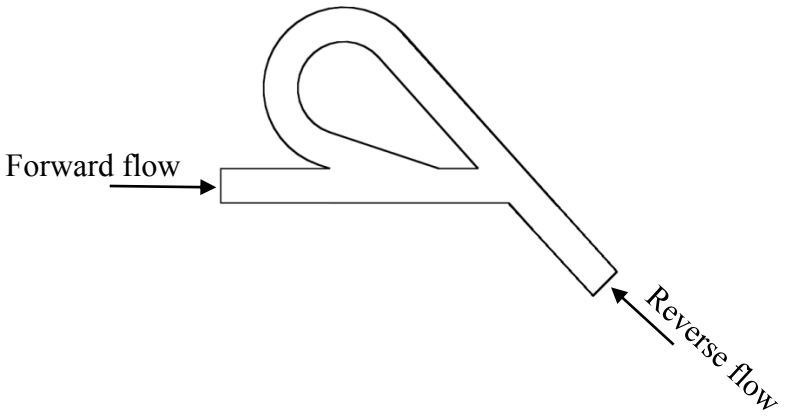

Figure 1.2 Tesla valve geometry with flow directions

Unlike the different geometries employed in micro-channels to increase heat transfer, the current study investigates potential of a Tesla valve (a check valve) to function as mini-to-micro-type heat exchanger along with its fluid rectification capabilities. An MSTV is formed using ten Tesla valves and is examined carefully using HPC for distinctive and periodic trends in fluid and thermal distributions. Pressure and thermal diodicity are used as criteria to determine the effectiveness of a MSTV for various operating conditions. Correlations for design parameters like Nusselt number, friction coefficient, pressure diodicity and thermal diodicity are derived.

CHAPTER II

LITERATURE REVIEW

In the 1990s, the Tesla valve was miniaturized and investigated for liquid flow control within microfluidic devices [9]. Ever since its microfluidics use was demonstrated, a number of computational and experimental studies have been performed to aid in valve design and for characterizing the mechanisms responsible for fluidic diode effects [9, 10, 12, 13, 14, 15, 17, 18, 31]. The performance of a Tesla valve, or any check valve, is measured by its diodicity, *Di*, which is the ratio of reverse and forward flow pressure drops across its structure. The *Di* depends on the application scale (micro or macro). Values between 1 and 2 [10] are reported for microscale applications while kinetic losses being dominant for macroscale applications result in *Di* values up to 4 [11].

Forster et al. may have first demonstrated the mini-to-microscale application of the Tesla valve [9]. By fabricating and experimentally characterizing a silicon Tesla valve prototype (100 μm square channel), termed the T45-R valve, they found that the Tesla valve *Di* increases linearly with flow rate for Reynolds numbers, Re, under 300, i.e. laminar flow [9]. Based on the T45-R design, Truong and Nguyen performed two-dimensional (2D), steady-state computational fluid dynamics (CFD) to further investigate flow behavior within the Tesla valve. For low Re, their simulation results, which were validated against experimental data provided by Forster et al. [9], were used for generating correlations for optimizing Tesla valve geometry for low Re [12]. Bardell

numerically and experimentally demonstrated that for low Re, Tesla valve diodicity depends on flow mechanisms such as viscous forces, laminar jets, high energy dissipation regions, and recirculation regions [10]. Zhang et al. by three-dimensional (3D) simulations on T45-R valve, found that a square channel yielded maximum Di for low Re (Re < 500), and a linear relationship was shown between aspect ratio and higher Re [13].

Gamboa et al. used non-dimensional design parameters to optimize the Tesla valve geometry for its use as a fixed-valve micropump. Based on the optimization, the return angle of the helix of the valve was found to be larger than the original valve introduced by Tesla. Increasing this angle resulted in helix flow opposing the main channel flow, in turn introducing a fluid velocity opposite to the pressure gradient in the main channel, an important factor for maximizing *Di*. This 'GMF' (i.e. Gamboa, Morris and Forster) valve proved to be 25 % more efficient than the T45-R valve design [14]. The *Di* obtained from 2D CFD was found to be significantly higher than experimental results.

Thompson et al. investigated the transitional and turbulent flow (Re < 2,000) within Tesla valves via 3D CFD [15]. Using Reynolds Averaged Navier Stokes (RANS) methods, numerical simulations were performed based on the k-Ɛ, k-k_L-ω and SST k-ω turbulence models. On implementing k-Ɛ model, Tesla valve flow could not be modelled accurately for the entire range of investigated Re. Unlike regular 2D CFD, k-k_L-ω and SST k-ω model results closely resembled experimentally measured *Di*. A concurrence was seen among the k-k_L-ω model and experimental data for Re up to 1,500. For Re = 2,000, experimental data was over predicted by k-k_L-ω and SST k-ω models.

The flow controlling effects imposed by a Tesla valve, like any passive-type check valve, can be amplified by spatially-arranging multiple valves in-series. Such valves provide an opportunity to increase *Di* significantly [16]. Thompson et al. evaluated the *Di* of MSTVs for laminar flow conditions by employing high performance computing (HPC) and 3D CFD [17]. Water being the working fluid, parameters like number of Tesla valve stages (up to 20), valve-to-valve distance (up to 3.375 hydraulic diameters), and Re (up to 200) were altered to study their effect on *Di* of MSTV. Previous experimental results validated the numerical results [14]. The diodicity of the MSTV was found to be proportional to Re and inversely proportional to valve-to-valve (G) distance. For low Re (i.e., Re < 50), the MSTV *Di* was shown to be independent of valve-to-valve distance and number of valves (N) used. Flow simulations done utilizing 3D CFD showed more accuracy than 2D CFD for a wide range of Re. For obtaining maximum *Di* with increasing Re, addition in the number of Tesla valves and minimization of valve-to-valve distance was suggested.

To study the mass transfer in micro-fluids, Mohammadzadeh et al. performed 3D, unsteady simulations on MSTVs for determining their flow-rectifying ability with pulsating flows at low or high frequencies [18]. This particular MSTV design consisted of 'high-angled' valve-to-valve connection schemes. Relative to nozzle-diffuser check valves, the investigated MSTVs displayed superior performance at higher frequencies. However, the nozzle-diffuser valve out-performed the MSTV at lower frequencies and Re.

Miniature or micro-sized channels, foundational structures of a Tesla valve, have been used for thermal management for quite some time [1]. Integrating fluids with target

thermal/fluidic properties with the high surface-area to volume ratio of mini/micro-channels allows for considerably high heat flux transport. With the reducing size of electronic equipment, consideration of micro-channels has gained importance [19]. Currently, heat sinks with micro-channels are a common application to enhance cooling from a small area [20]. Many have implemented new design concepts for increasing the heat transfer capability of mini-to-micro-sized channels. Heat transfer enhancement of micro-channel, due to limitations in working fluid properties, is typically constrained to micro-channel design features.

Hsiao et al. used a T-shaped channel with rectangular winglet pairs (RWPs) for micro-mixing applications [21]. The performance dependence of micro-mixers with micro-scale Longitudinal Vortex Generators (LVGs) on design parameters was investigated. Results indicated enhanced heat transfer capability and fluid mixing throughout the T-shaped channel when using angled RWPs due to longitudinal vortices generation. Addition of divergent RWPs to micro-mixers enhanced the performance of micro-mixers. Integration of the RWPs provides a means to induce swirl-type flows, and thus increased heat transfer and mixing, as a result of them functioning as in-channel obstacles.

Karale et al. investigated the dependence of heat transfer on geometrical parameters in series serpentine channels (10 channels) [22]. Dependence of design parameters on Re was found. Lee et al. used numerical simulations to study the interaction of two synthetic jets under cross-flow condition in a micro-channel [23]. Out-of-phase flow configuration proved more thermally efficient in comparison to in-phase-flow configuration. Wang et al. [24] used pillars in micro-channels to enhance the heat

transfer capability. Using air as the working fluid, the heat transfer coefficient was seen to increase twice its value.

Sui et al. compared the Nusselt number, Nu, and friction factor, *f*, of wavy micro-channels (width = 205 μm and depth = 404 μm) to straight baseline channels with similar cross-section and foot print length for 300 < Re < 800 [25]. Imbalance in the pressure gradient close to wall surface causes secondary flows resulting in the spatial evolution of Dean vortices, leading to chaotic advection within the channel. This increased the heat transfer performance of the wavy channels in comparison to the straight channels with a very low pressure drop penalty.

Xie et al. numerically studied the effects of Re (100 < to Re < 900), and arrangement patterns in a rectangular microchannel (height = 100 μm and width = 20 μm) with dimples/protrusions. Increase in the heat transfer performance with a low pressure drop penalty was demonstrated in comparison to conventional channels. Flow reattachment and shedding of vortices caused high heat transfer region in downstream portion of dimple and dimple wake whereas flow separation resulted in low heat transfer region on the upstream portion of dimple [26].

Che et al. analytically studied the heat transfer in microchannels employing plug flow. The results exhibited high Nu and heat transfer indices for short plugs, displaying notable heat transfer. Transverse component of velocity increased recirculation of flow leading to enhancement in the transport of fresh fluid and heated fluid between the center and the wall of plug, thus increasing heat transfer [27].

Ebrahimi et al. used a non-uniform DC electric potential and zeta potential on horizontal and ribbed channels to study the mixing and heat transfer enhancement. A

Schmidt number value for every Re was noted, below which mixing was affected negatively by the electric field. [28].

Peles et al. utilized a microscale pillar in a microchannel to enhance heat transfer. Flows in a plain microchannel, a microchannel with pillar, and a microchannel with a jet were studied. Increase in heat transfer was noticed on addition of pillar and secondary jet. Eighty percent enhancement in spatially averaged Nusselt number was obtained at a Reynolds number of 730 [29].

Morini et al. critically analyzed the factors affecting forced microconvection of liquid and gas flows through microchannels. Besides scaling and micro-effects, factors like geometry of test rig, real thermal boundary conditions, and presence of fittings, positions, and type of sensors played a major role in determining convection coefficient [30].

Thompson et al. used Tesla valves in flat plate oscillating heat pipe (FP-OHP) to increase heat transfer [31]. Neutron radiography and image analysis techniques were used for flow visualization and motion tracking. A circulatory flow was seen due to flow rectification by Tesla valves. Addition of heat led to intensification of the diodicity of the valves.

CHAPTER III

PROBLEM SETUP

3.1 Computational Geometry and Flow Condition.

A GMF Tesla valve [10] with a square cross section and hydraulic diameter, D_{H} = 1 mm, and design and forward/reverse flow directions shown in Fig. 3.1, was numerically investigated for this study using CFD. The GMF Tesla valve was investigated due to its near-optimal trunk (originating artery) and helix (bifurcating artery) designs for laminar flow. To ensure that hydrodynamically fully-developed flow entered the Tesla valve (in forward or reverse flow directions), Eq. (3.1) was used to calculate the hydrodynamic entrance length, δ, i.e.:

$$\delta = 0.05\mathrm{Re}D_{\mathrm{H}} \tag{3.1}$$

For Re = 200, which is the maximum Re investigated herein, δ of 10 mm was calculated and extra length entrance length added to the Tesla valve was twice the calculated hydrodynamic length as shown in Fig. 3.1. Minimizing the valve to valve distance for superior performance as suggested by Thompson et. al [17], a constant valve-to-valve distance (1mm), a ten-staged MSTV, i.e. N = 10, was formed by arranging valves in-series as shown in Fig. 3.2.

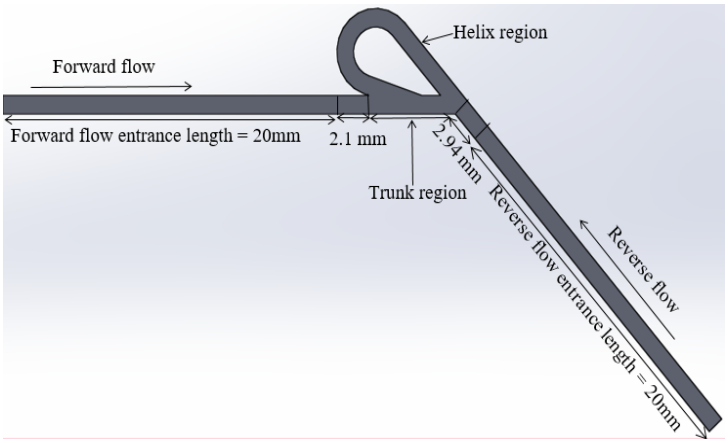

Figure 3.1 Schematic of single GMF Tesla valve with flow directions and dimensions

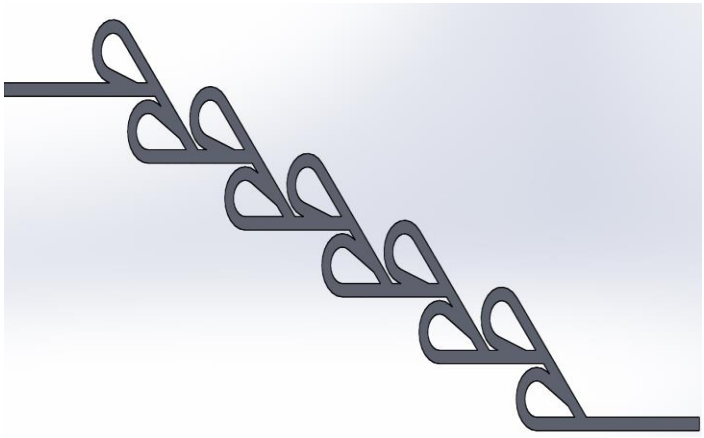

Figure 3.2 A MSTV based on the GMF valve design (N = 10)

The Re was varied between 25 and 200 in order to investigate its effects on the *Di* of the MSTV.The temperature was chosen arbitrarily to ensure that fluid exiting MSTV is at higher temperature than the walls, so heat transfer could be calculated.

3.2 Evaluation Criteria

The effectiveness of the Tesla valve in functioning as either a fluidic or thermal diode is determined by measuring the pressure and temperature difference across the Tesla valve during each flow direction, respectively. For each case, a pressure diodicity,

Di_P, and thermal diodicity, Di_T, were defined. Pressure diodicity (Di_P) was defined as the ratio of pressure drops in the reverse and forward direction, i.e.:

$$Di_P = \frac{\Delta P_r}{\Delta P_f} \tag{3.2}$$

Similarly, Di_T was defined as the ratio of Nu in the reverse and forward flow direction, i.e.:

$$Di_T = \frac{Nu_r}{Nu_f} \tag{3.3}$$

Along with these non-dimensional quantities, correlations for the Nu, Di_P, Di_T and f, as functions Re were extracted from the numerical results by using nonlinear modelfit function in Mathematica The coefficient of determination was measured to be more than 0.99 at all times for accuracy. To account for flow variation along the MSTV, aforementioned evaluation criteria were applied to the first and last MSTV valve.

3.3 Solution Method

The 3D flow through the Tesla valve was assumed to be (1) at steady state; (2) incompressible; (3) laminar; (4) with constant fluid properties; (5) with negligible viscous dissipation; (6) with no slip condition; (7) single phase flow and (8) with negligible gravity effects (flow perpendicular to gravity). The governing equations for fluid continuity, momentum and energy are stated in Eq. (3.4) - (3.6), respectively. These equations were solved for the fluid steady-state velocity field, $\boldsymbol{u}$, and steady-state temperature field, T.

$$\frac{\partial u_j}{\partial x_j} = 0 \tag{3.4}$$

$$\rho u_j \frac{\partial u_l}{\partial x_j} - \mu \frac{\partial^2 u_l}{\partial x_j \partial x_j} + \frac{\partial P}{\partial x_l} = 0 \tag{3.5}$$

$$\frac{\partial[u_j(\rho E+P)]}{\partial x_j} = \frac{\partial[k_{eff}\frac{\partial T}{\partial x_j} + u_l \tau_{eff,l,j}]}{\partial x_j} \quad (3.6)$$

For Eqs. (3.4) - (3.6), k_{eff} is the effective conductivity, τ_{eff} is the effective viscous dissipation, and E is the total energy (sum of thermodynamic internal energy e and bulk kinetic energy $u^2/2$). The boundary conditions utilized for Eqs. (3.4) - (3.6) consisted of (i) no-slip along the channel wall, (ii) uniform velocity at inlet, (iii) a pressure outlet and (iv) isothermal wall temperature of 20 ºC. These equations were numerically solved by employing a pressure based finite volume double precision 3D solver via ANSYS FLUENT (v. 14.5.7).

An unstructured tetrahedral grid with uniform cell density was generated (GAMBIT, v. 12), with a typical mesh shown in Fig. 3.3. The SIMPLE algorithm and momentum-weighted interpolation scheme were used to solve the pressure-velocity coupling, and pressure discretization, respectively. The Second Order Upwind scheme was applied to discretize the momentum and energy equations. Three to five thousand iterations along with no convergence criteria were ran for every simulations to let the simulations reach convergence by its own. Convergence for momentum and energy was determined based on the reduction of residuals to five orders of magnitude. High performance computing (HPC) was utilized to efficiently and effectively perform the numerical investigation.

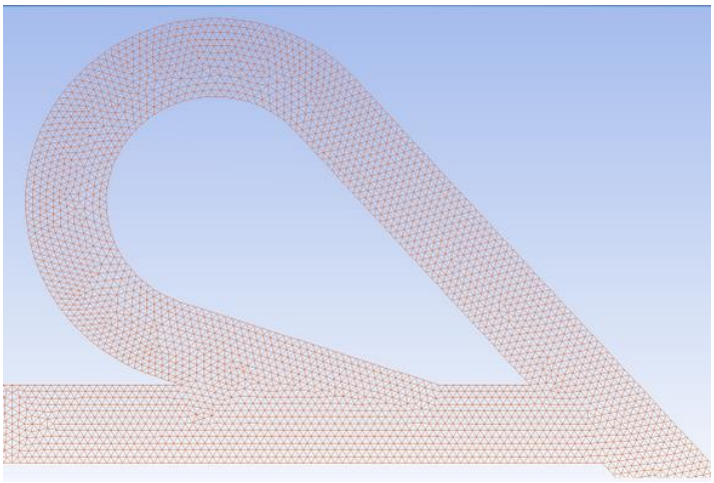

Figure 3.3 Unstructured tetrahedral mesh generated using GAMBIT

3.4 Data Analysis

Velocity at the inlet was prescribed based on a target Reynolds number, Re, defined as:

$$\mathrm{Re} = \frac{\rho u_{\mathrm{i}} D_{\mathrm{H}}}{\mu} \tag{3.7}$$

where u_i is the average velocity at the inlet and D_{H} is the hydraulic diameter, which for the square cross section investigated is 1 mm. From the obtained temperatures at the inlet and outlet of the Tesla valve, the average heat transfer rate was calculated using Eq. (3.8).

$$q = \dot{m} c_{\mathrm{p}} \Delta \mathrm{T} \tag{3.8}$$

Mass flowrate $\dot{m}$ was calculated using fluid properties at the inlet by Eq. (3.9).

$$\dot{m} = \frac{\pi \mathrm{Re} D_{\mathrm{H}} \mu}{4} \tag{3.9}$$

The resulting heat rate was used to determine average heat transfer coefficient ($\bar{h}$) through log-mean temperature difference method. Eq. (3.10) was applied to deduce the average heat transfer coefficient ($\bar{h}$).

$$\bar{h} = \frac{q}{A_c \Delta T_{LM}} \tag{3.10}$$

Here A_c is the cross-sectional area at the entrance of the Tesla valve and ΔT_{LM} is the log-mean temperature difference found from Eq. (3.11), i.e.:

$$\Delta T_{LM} = \frac{(T_w - T_o) - (T_w - T_i)}{\ln[(T_w - T_o)/(T_w - T_i)]} \tag{3.11}$$

where T_w, T_i, T_o are wall, bulk mean inlet and outlet temperatures, respectively. The average heat transfer coefficient was utilized to calculate the average Nusselt number, $\overline{Nu}$, using Eq. (3.12), i.e.:

$$\overline{Nu} = \frac{\bar{h} D_H}{k} \tag{3.12}$$

This $\overline{Nu}$ was calculated for various Re for forward and flow directions to determine the Di_T described in Eq. (3.3). Using the pressure difference, the Darcy friction factor ($\bar{f}$) was determined by Eq. (3.13).

$$\bar{f} = -\frac{(\Delta P) D_H}{\rho u_i^2/2} \tag{3.13}$$

The pressure diodicity (Di_P) was obtained by using the total pressure difference recorded at the inlet and outlet of Tesla valves as shown in Eq. (3.2).

3.5 Mesh Independence and Validation Study

The numerical solutions for *Di* were inspected for mesh independence. This was accomplished by performing four distinct simulations with meshes of varying resolution for the scenario: $N = 20$, $T_i = 80$ °C and Re = 200 with water as the working fluid. The

results of the mesh independence study are presented in Fig. 3.4. It can be seen that, in general, there was less than a 1% change in *Di* with increasing mesh resolution. Based on these results, an approximate mesh resolution of 130,000 cells per Tesla valve was selected for the entire study of this paper.

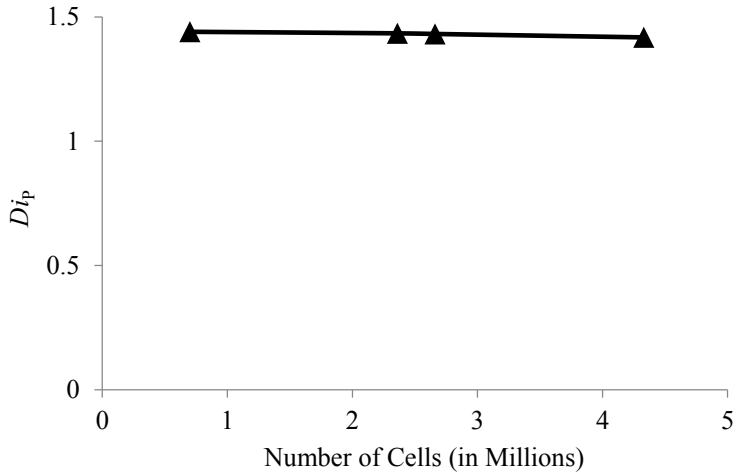

Figure 3.4 Diodicity vs. number of cells (in millions) for MSTV with N = 20, Re = 200, T_i = 80ºC

To evaluate the accuracy of the methodology used to calculate $\overline{Nu}$, numerical simulations were performed using circular and rectangular channel of arbitrary cross-sections. Periodic boundary conditions were used to ensure fully developed flow in each of the channels. Keeping the inlet temperature (T_i = 80 °C), wall temperature (T_w = 20 °C), and fluid properties constant, simulations were performed for Re = 75, 100, 150, 200 with water as the fluid. Average fluid temperatures were extracted from fictitious cross-sectional planes (normal to inlet flow direction) located at approximately 30% and 70% of the total channel length. This was done to avoid edge effects that influenced the

temperature profile at the entrance and exit of the channels. The average Nusselt numbers determined via simulation and using Eq. (3.12) were compared to empirically-predicted, average Nusselt numbers [32] for flow within an isothermal duct Eq. (3.14), or isothermal tube, Eq. (3.15), i.e.:

$$\overline{\mathrm{Nu}}_{\mathrm{cir}} = 3.66 \tag{3.14}$$

$$\overline{\mathrm{Nu}}_{\mathrm{sq}} = 2.98 \tag{3.15}$$

As shown in Fig. 3.5, $\overline{\mathrm{Nu}}$ agrees very well with empirically-calculated values within 1 % error for both circular and square channels

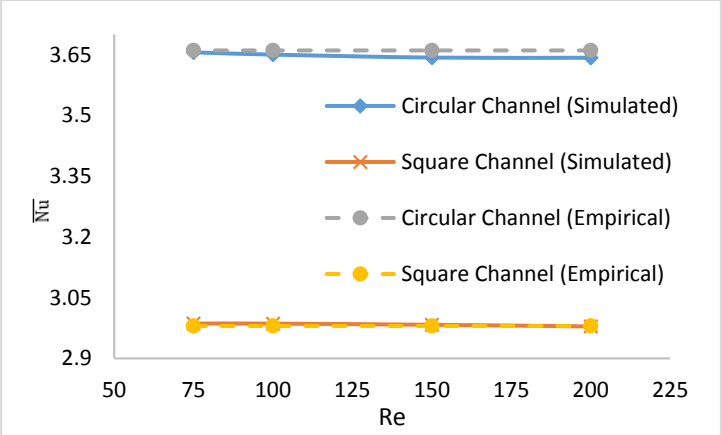

Figure 3.5 Simulated and empirically-predicted $\overline{\mathrm{Nu}}$ vs. Re for circular and square tubes

CHAPTER IV

RESULTS AND DISCUSSION

4.1 Fictitious plane setup for result extraction

Total pressure and average/static temperature was extracted from fictitious, cross-sectional planes located along the MSTV structure. A part of MSTV with planes is shown in Fig. 4.1(planes 1-11). Preliminary analysis indicated that the momentum and temperature varied with respect to the MSTV length; i.e. between the first Tesla valve and 'downstream' valves. Hence, in order to capture this asymmetry in flow/temperature along the MSTV structure, the first and last valves (for a given flow direction) were analyzed – corresponding to the 1^{st} and 10^{th} valves encountered for either forward or reverse flow direction within a ten-staged MSTV. As shown in Fig. 4.1, these planes were equally spaced from each valve; with planes in between two valves acting as the exit to one valve and entrance to another. Planes a through d in Fig. 4.1 provide a close-up view of plane locations for determining the mass flow rate distribution in a single Tesla valve. For the purpose of comparing trunk and helix flow characteristics, planes shown in Fig. 4.2 were imposed for data extraction.

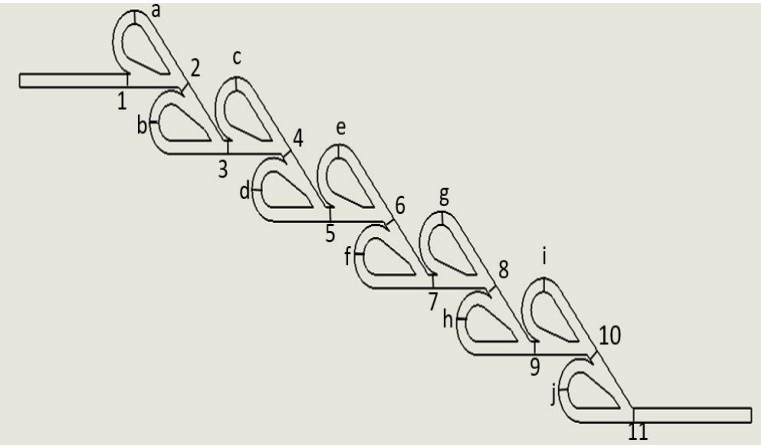

Figure 4.1 Fictitious plane location for extraction of pressure, temperature and mass flow rate data

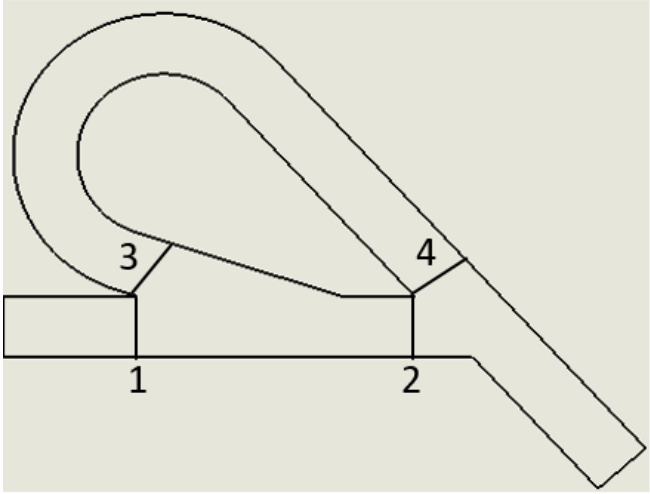

Figure 4.2 Fictitious planes for helix and trunk of Tesla valve

4.2 Comparative Study

The flow behavior and heat transfer within the MSTV (N = 10, forward and reverse flow) and conventional square micro-channel (having similar volume as MSTV) were compared. All simulations were performed using water with Re = 200, T_i = 80 ºC

and T_w = 20 ºC. Parameters were extracted from the fictitious planes drawn inside conventional channel (at equivalent points as planes 1-11 in Fig.4.1) The comparison between the average pressure and temperature profile along the MSTV length is shown in Fig. 4.3. It may be seen from Fig. 4.3(a) that pressure drop is the lowest in the case of straight channel whereas reverse flow in the MSTV accounts for the highest pressure drop with respect to length. This is a result of the unique Tesla valve geometry which promotes a higher pressure drop during reverse flow due to complex flow phenomena at the helix inlet and outlet, i.e.: jet impingement, bifurcation and backflow.

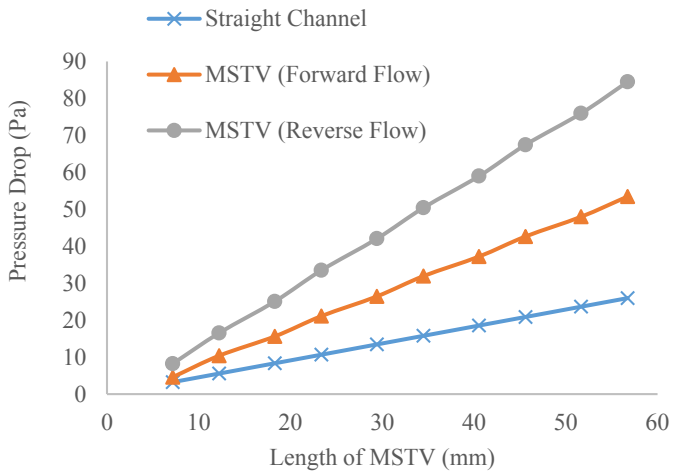

a

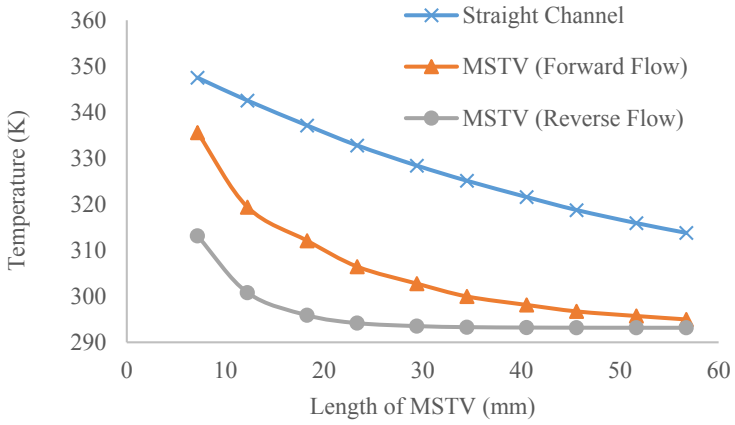

b

Figure 4.3 Numerical results from plane locations (1) – (10) for Forward and/or reverse flow through straight square cross-sectioned channel and MSTV: (a) pressure drop and (b) temperature.

The trend for heat transfer capability is completely opposite as for pressure drop (Fig. 4.3(b)). As shown in Fig. 4.3(b) highest heat transfer (per unit length) was seen for reverse flow of MSTV, followed by forward flow of MSTV and straight channel. To explain the trend of heat transfer enhancement, flow distribution in the Tesla valve was

studied. It was found that with an increase in Re, the mass flow percentage in the Tesla valve helix increased for reverse flow, whereas it decreased for forward flow. Fig. 4.4(a) and 4.4(b) display this behavior for both cases. For forward flow, at higher Re (RE>100), it is seen that mass flow in even number of valves is higher than the odd number valves. This is due to the unique arrangement of Tesla valves in the MSTV and small valve to valve distance (G). Flow coming down the odd number of valves hits the walls at an incline angle resulting in increased backflow, causing higher percentage of fluid entering the helix of even number valves. The second valve receives the highest mass flow (as shown in Fig. 4.4(a)) in helix region because the velocity of flow coming from first valve is the highest along MSTV.

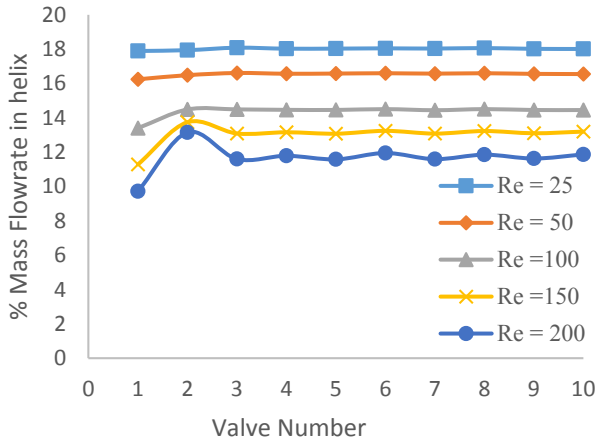

a

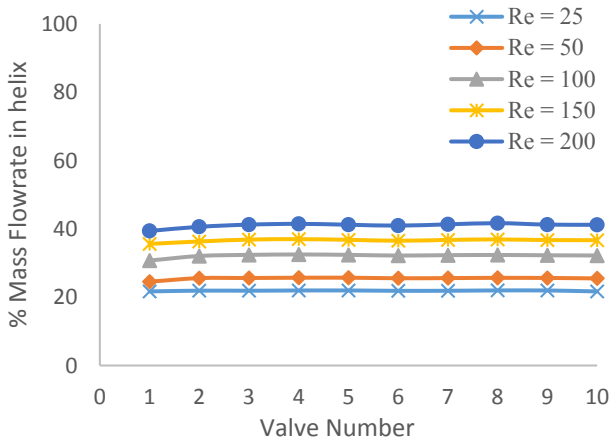

b

Figure 4.4 Valve Number vs % mass flow rate

a) Forward Flow b) Reverse Flow

To better understand Tesla valve thermal performance, the planes shown in Fig. 4.2 were drawn for the first valve in case of forward flow. Planes 1 & 2 measured the temperature of flow entering and exiting the trunk of Tesla valve whereas the planes 3 & 4 accounted for the helix. A temperature difference based on the flow temperature entering and exiting the trunk and helix part of Tesla valve was measured. A percentage

reduction in temperature was calculated based on the inlet temperature at different Re and plotted in Fig. 4.5.

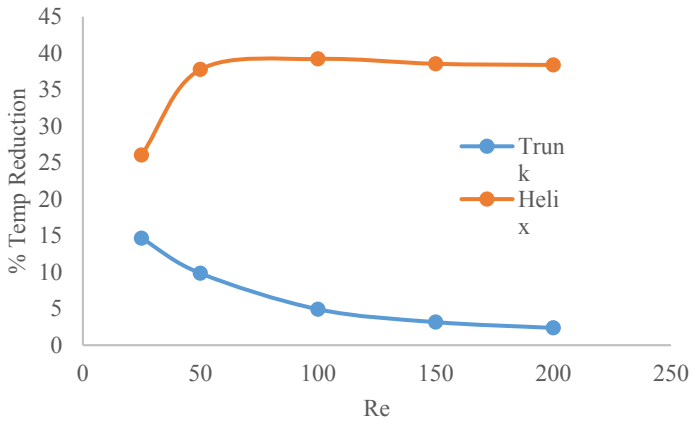

Figure 4.5 Percent temperature reduction along the helix and trunk parts of a Tesla valve

It was found that heat transfer in the Tesla valve helix is much higher compared to its trunk. With an increase in Re, steady percentage temperature reduction was noticed in the helix whereas it reduced for the trunk. Thus, the results demonstrate that the heat transfer of the MSTV is enhanced during reverse flow due, in part, to the higher mass flow-rate in the Tesla valve helixes.

Surface area plays an important role in heat transfer. Although the surface area of MSTV is higher compared to straight channel there are other different factors that contribute majorly to increasing thermal enhancement capability in either the forward or reverse flow directions. One such factor is formation of stationary transverse vortices at the junction of flow bifurcation (Fig. 4.6(a)) during forward flow in Tesla valve. Flow becomes unsteady locally due to presence of vortices leading to heat transfer

enhancement by means of 'Reynolds' averaged transport [33]. Stationary transverse vortices aid to heat transfer by convectively transporting energy from the fluid center to wall and vice versa. Other factors supplementing heat exchange in reverse flow is jet impingement and flow mixing near the helix outlet. The stagnation region of impingement and flow mixing region are shown in Fig. 4.6 (b).

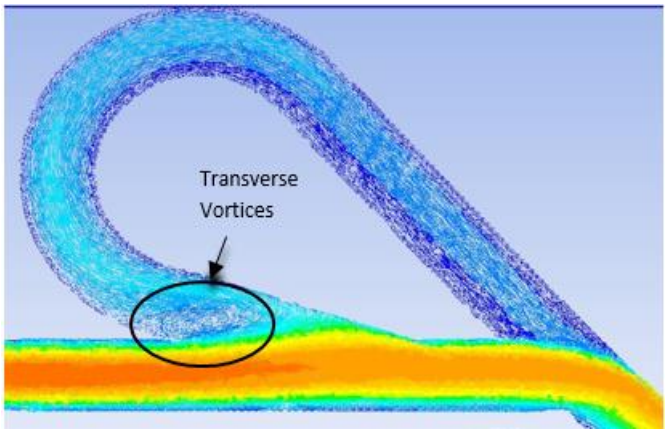

a

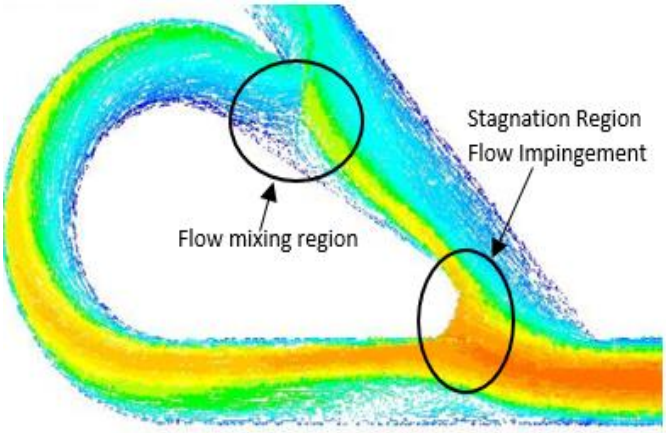

b

Figure 4.6 a) Transverse vortices formation in forward flow b) Flow Impingement and Flow mixing regions in reverse flow

4.3 Friction Coefficient Correlation

From the pressure data extracted from the planes (1-11) shown in Fig. (4.1), the friction factor for flow within each Tesla valve was calculated using Eq. (3.13). This procedure was repeated for different Re for both forward and reverse flow. The plots are shown in Fig. 4.7(a) & (b).

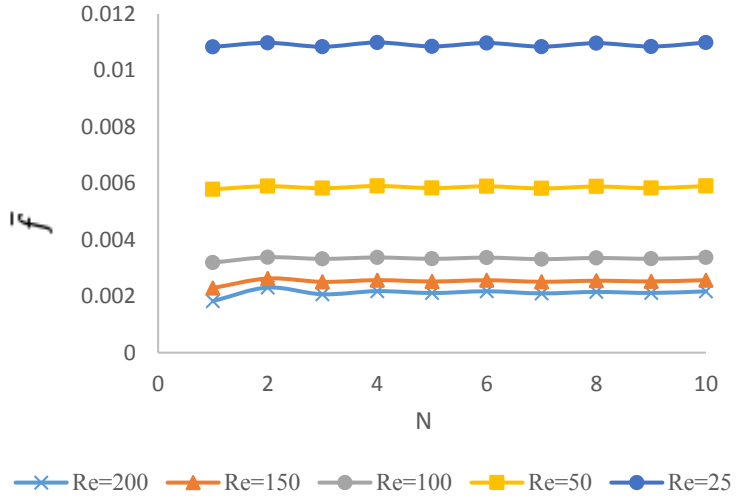

a

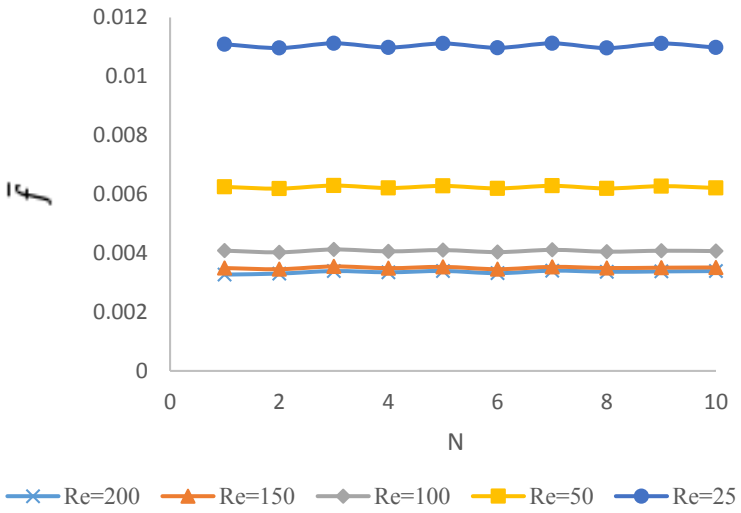

b

Figure 4.7 Average Friction factor vs. Valve number

a) Forward flow b) Reverse Flow

The results indicate that the friction factor increases with lower Re; for the case of Re = 25, the average friction factors were 0.01091 & 0.01104 for forward and reverse

flow, respectively. The lowest average friction factors of 0.00212 & 0.00335 were observed for Re = 200 during forward and reverse flow, respectively. A running average (average over different number of valves together) of Tesla valves against Reynolds number is plotted for both forward and reverse flow in Fig. 4.8(a) and (b). These plots indicate the average over a different N. A maximum average friction factor value of about 0.12 is reached in both cases for Re = 25.

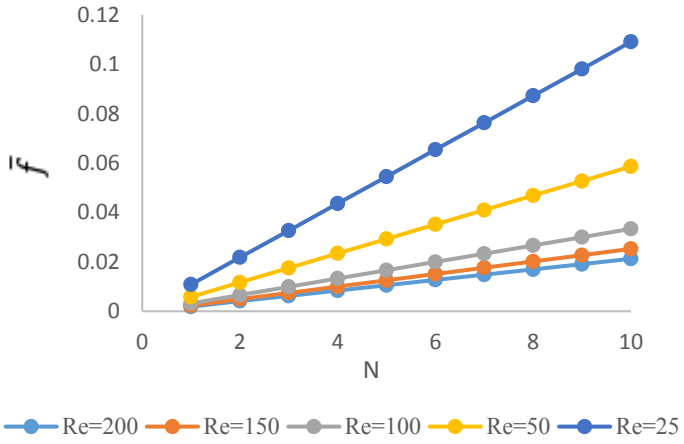

a

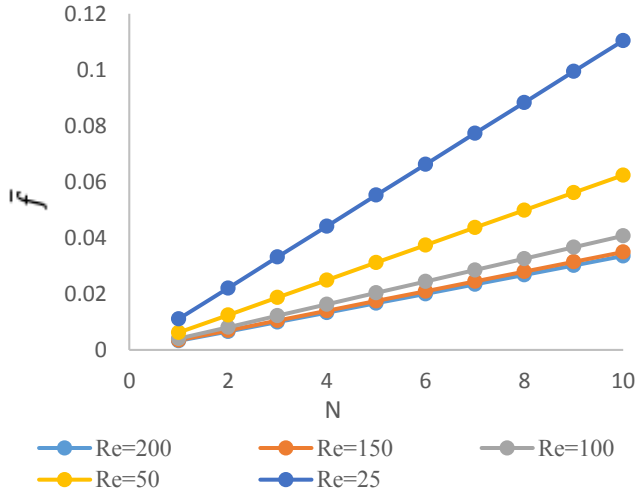

b

Figure 4.8 Running average friction factor vs. N

a) Forward flow b) Reverse Flow

The average friction factors for the first and last valve of the MSTV were plotted against Re, as shown in Fig. 4.9(a) & (b), to aid in generating empirical correlations for MSTV design.

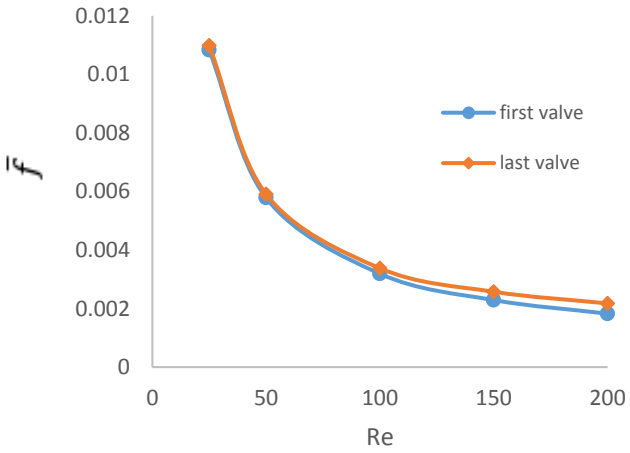

a

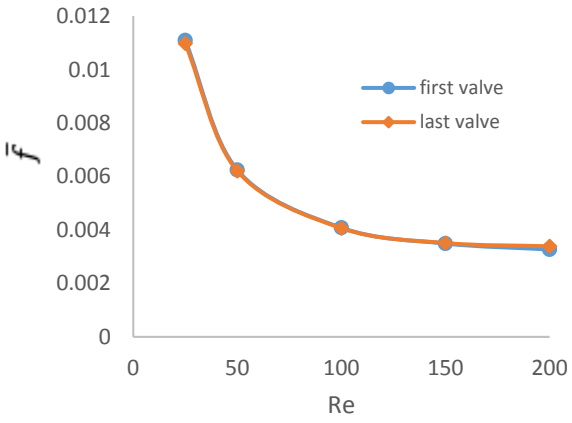

b

Figure 4.9 Average friction factor vs. Re for first and last valve

a) Forward flow b) Reverse Flow

Equation (4.1) and (4.2) contains correlations of first and last valve for forward flow whereas Eq. (4.3) and (4.4) contain correlations for reverse flow.

$$\bar{f}_{1,\text{fwd}} \cong 0.180742(\text{Re}^{0.876}) \quad (4.1)$$

$$\bar{f}_{\infty,\text{fwd}} \cong 0.156781(\text{Re}^{0.828}) \quad (4.2)$$

$$\bar{f}_{1,\text{rev}} \cong 0.0912696(\text{Re}^{0.663}) \quad (4.3)$$

$$\bar{f}_{\infty,\mathrm{rev}} \cong 0.0863161(\mathrm{Re}^{0.649}) \tag{4.4}$$

4.4 Pressure Diodicity Correlation

Using Eq. (3.2), the pressure diodicity for every Tesla valve within the MSTV was calculated. The variation of pressure diodicity along the length of MSTV is shown in Fig. 4.10 (a).

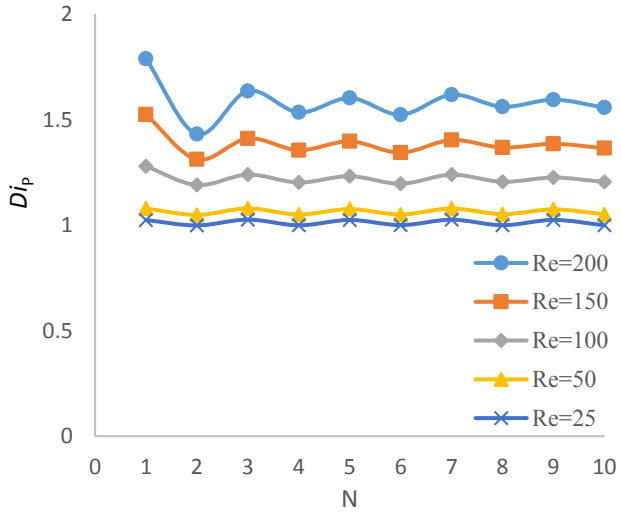

a

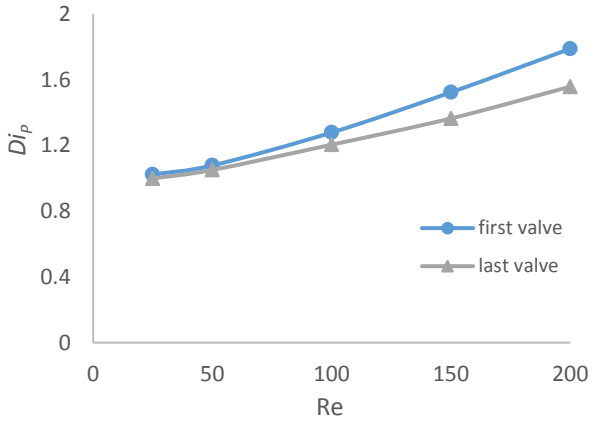

b

Figure 4.10 a) Di_P vs. Valve no b) Di_P vs. Re for first and last valve

An increase in Di_P is seen as Re is increased, with Re = 200 having the highest values of Di_P. Change in Di_P with increasing Re for first and last valve is shown in Fig. 4.10 (b). It is inferred from the data that for Re > 100, first valve displays higher diodicity. With a data curve fit, correlations of Di_P in terms of Re were derived for both the first and last valves, i.e. Eq. (4.5) and (4.6), respectively.

$$Di_P \cong 0.975 + 0.000435(\mathrm{Re}^{1.422}) \tag{4.5}$$

$$Di_P \cong 0.958 + 0.000574(\mathrm{Re}^{1.312}) \tag{4.6}$$

4.5 Nusselt Number Correlation

Temperature data obtained from planes (1-11) in Fig. 4.1 was used to produce $\overline{\mathrm{Nu}}$ for every valve using Eq. (3.12). For forward and reverse flows, $\overline{\mathrm{Nu}}$ variation along MSTV can be seen in Fig. 4.11 (a) and (b) respectively.

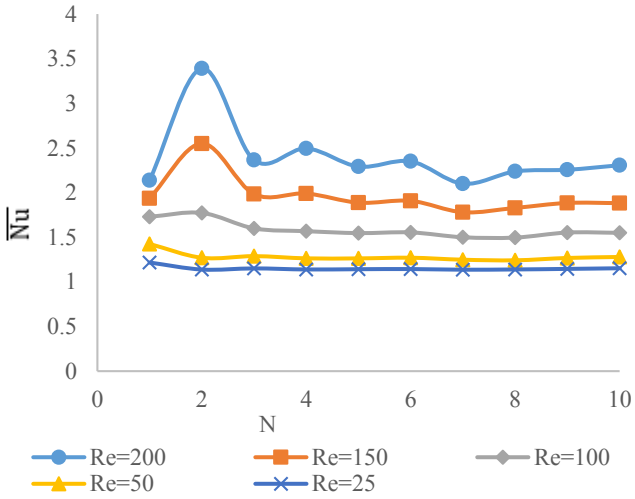

a

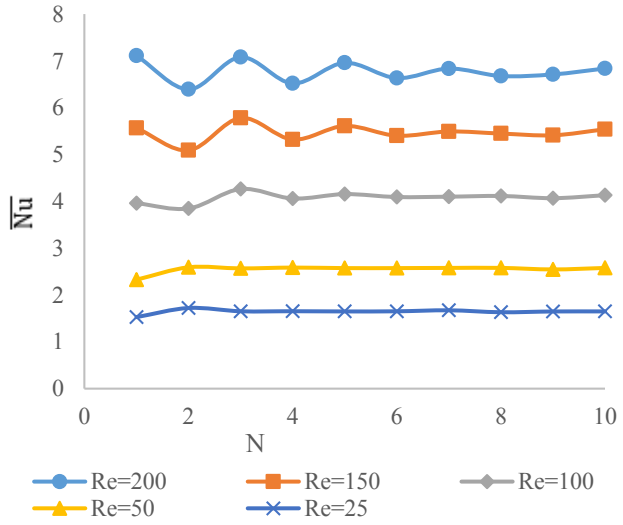

b

Figure 4.11 Average Nusselt number vs. Valve number

a) Forward flow b) Reverse Flow

Higher fluctuations can be seen amongst the initial valves compared to the latter part of MSTV. A bulge in the average $\overline{Nu}$ trend of forward flow is seen in Fig. 4.11 (a) for the second valve. This sudden spike is due to the higher mass flow-rate in helix (shown in Fig. (4.4)) for second valve which enhanced the thermal efficiency of this

valve resulting in higher $\overline{Nu}$. Fig. 4.12 (a) & (b) contain the $\overline{Nu}$ running average over different number of Tesla valves. Eventually as the number of valves (N) are increased for both cases, the periodic behavior is observed and a steady state $\overline{Nu}$ value is attained for different Re.

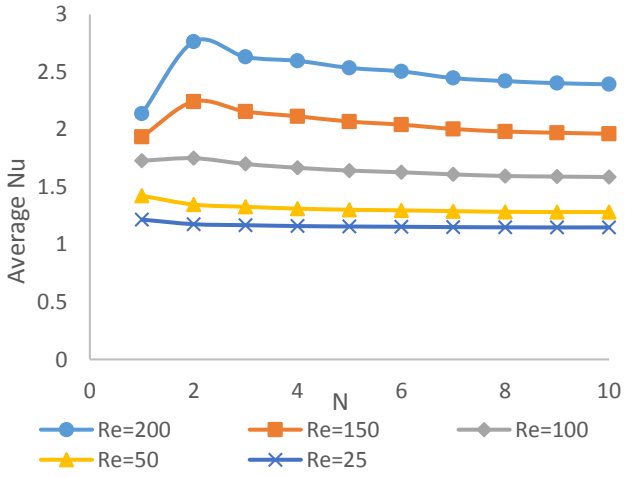

a

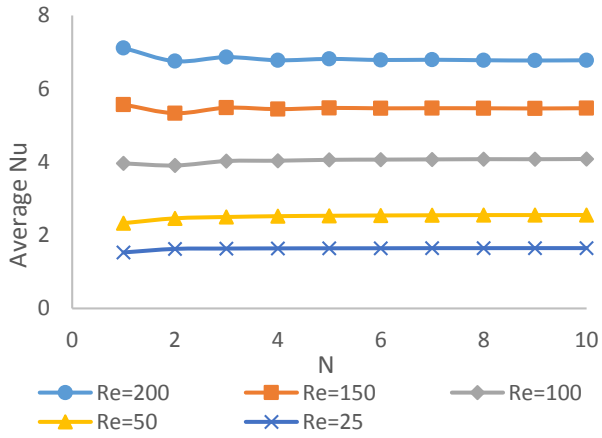

b

Figure 4.12 Running average Nusselt number vs. N

a) Forward flow b) Reverse Flow

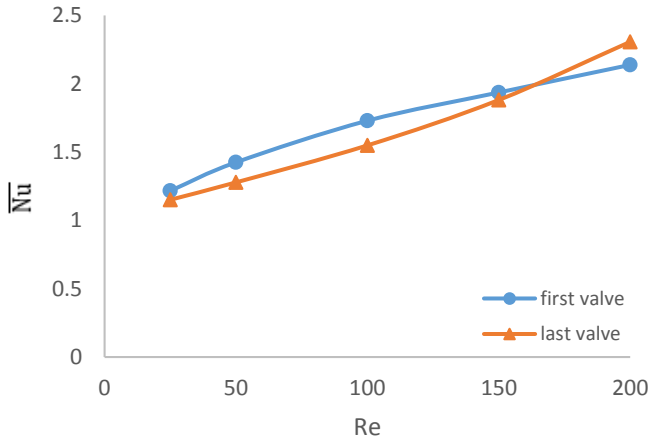

a

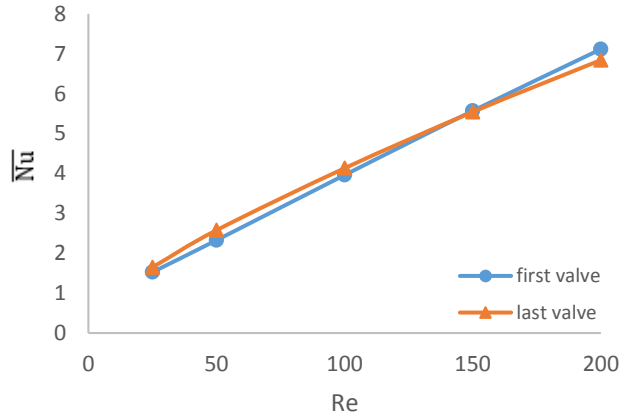

b

Figure 4.13 Average Nusselt number vs. Re for first and last valve

a) Forward flow b) Reverse Flow

Change in $\overline{Nu}$ with an increase in Re for the first and last valve are shown in Fig. 4.13 (a) and (b). $\overline{Nu}$ is observed to have a high dependence on Re. Increasing Re produces a positive gradient in $\overline{Nu}$ trends for both valves. Application of non-linear curve fit model produced correlation of $\overline{Nu}$ as a function of Reynolds number (Re) and Prandlt number (Pr). Correlations for first and last valve for forward flow are mentioned in Eq. (4.7) and (4.8) whereas Eq. (4.9) and (4.10) contain correlations for reverse flow.

$$\overline{\mathrm{Nu}}_{1,\mathrm{fwd}} \cong 0.126\mathrm{Re}^{0.276}\mathrm{Pr}^{1/3} \tag{4.7}$$

$$\overline{\mathrm{Nu}}_{\infty,\mathrm{fwd}} \cong 0.167\mathrm{Re}^{0.361}\mathrm{Pr}^{1/3} \tag{4.8}$$

$$\overline{\mathrm{Nu}}_{1,\mathrm{rev}} \cong 0.056\mathrm{Re}^{0.789}\mathrm{Pr}^{1/3} \tag{4.9}$$

$$\overline{\mathrm{Nu}}_{\infty,\mathrm{rev}} \cong 0.087\mathrm{Re}^{0.699}\mathrm{Pr}^{1/3} \tag{4.10}$$

4.6 Thermal Diodicity Correlations

Based on the $\overline{\mathrm{Nu}}$ values derived in the previous section, Thermal diodicity (Di_T) was determined by applying Eq. (3.3). The difference in Di_T along the length of MSTV is shown in Fig. 4.14(a).

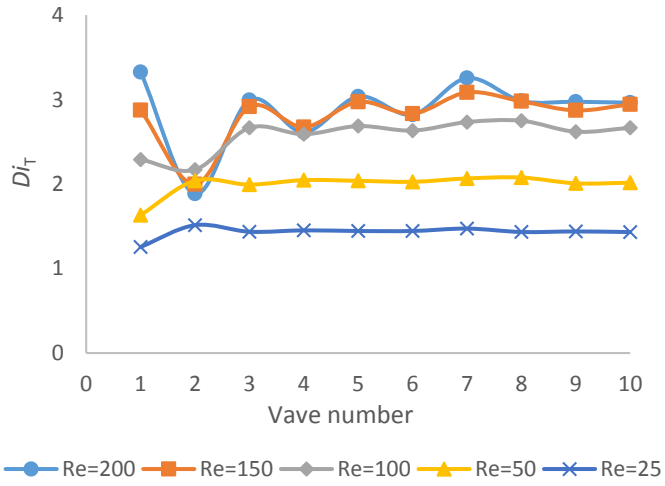

a

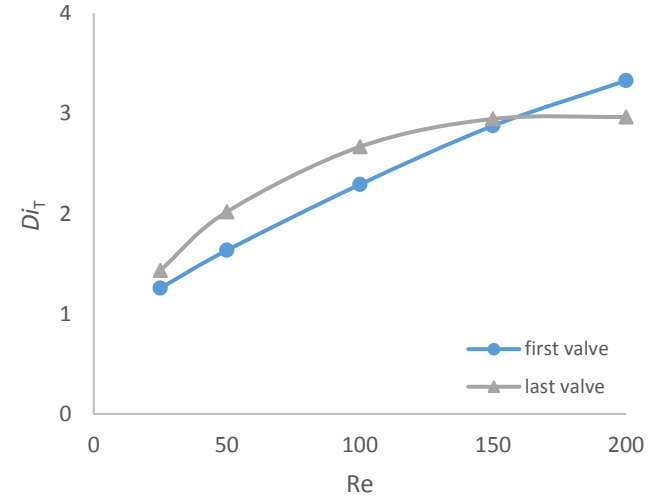

b

Figure 4.14 a) Di_T vs. Valve no b) Di_T vs. Re for first and last valve

Di_T trends are seen to fluctuate more for Re > 100. The deeper depressions in the trends for Re = 150 & 200 are due to higher mass flow-rate entering the second valve. To evaluate correlations for the first and last valve as a function of Re, Di_T was plotted against Re as shown in Fig. 4.14(b). It is observed that there is almost a linear increase in Di_T for the first valve whereas a fully developed value is reached for the last valve at Re

= 150. Correlations derived for the first and last valve using curve fitting techniques are shown in Eq. 4.11 and 4.12, respectively.

$$Di_{\mathrm{T}} \cong 0.59 + 0.072(\mathrm{Re}^{0.69}) \tag{4.11}$$

$$Di_{\mathrm{T}} \cong 0.54(\mathrm{Re}^{0.33}) \tag{4.12}$$

CHAPTER V

CONCLUSION AND FUTURE WORK

5.1 Conclusion

Application of CFD techniques has not only helped in studying the diodic effect but also brought into light the thermal enhancement capabilities of Tesla valves. Addition of 20 mm entrance length ensured that hydro-dynamically fully developed flow entered the MSTV (N = 10). Keeping constant fluid properties, Re was varied to study the fluid rectification and heat transfer capability of different number of Tesla valves. Correlations for friction coefficient, pressure diodicity, Nusselt number and thermal diodicity were calculated. Most important conclusions include:

1. With a penalty of higher pressure drop, astonishing decrease in fluid temperature was noted for reverse and forward flow of MSTV compared to using a straight channel.
2. Differences in the flow behavior were seen of the first and last valve of MSTV
3. Periodicity in flow and thermal distributions was noticed along the later half of MSTV.
4. It was seen that increasing Re leads to a reduction in friction factor and pressure diodicity values along the length of MSTV.
5. Nusselt number values for reverse flow were calculated to be almost two times the values for forward flow.
6. Nusselt number and thermal diodicity reach fully developed values for flow with Re= 150 and higher.

7. Anomalies in pressure difference are observed between a single Tesla valve and a two-staged MSTV, and this anomaly becomes more exaggerated with higher Re. Higher flow velocity, unique MSTV arrangement and small G account for this anomaly.

8. Given a specific value of Re and G, the above derived correlations can be applied for using Tesla valves in different applications. Correlations for the first valve should be used along with last valve correlations for additional valves for designing an MSTV.

5.2 Future work

In this study thermal enhancement capability of Tesla valve was explored. Multistage Tesla valve (MSTV) was made by arranging Tesla valves in series. It addition, correlations for friction coefficient, pressure diodicity, Nusselt number and thermal diodicity were derived for design purposes. Future research work will focus on enhancing the design of Tesla valve and making structural modifications on the interior surface to enhance mixing and keeping a continuous development of thermal boundary layer. It will also explore the effect of varying valve to valve distance on different correlations. Also, Tesla valves are used only at micro or mini scale until today, its use at macro scale is another application to be explored.

REFERENCES

1) Tuckerman, DB., Pease, RFW., 1981," High-performance heat sink for VLSI", *IEEE Electron Device Lett* , **2,** pp. 126-129.

2) Mehendale, S.S., Jacobi, A.M., Shah, R.K., 2000, "Fluid flow and heat transfer at micro-and meso-scales with application to heat exchanger design", *Applied Mechanics Review*, **53**, pp. 175-193.

3) Kandlikar, S.G., Grande, W.J., 2002, "Evolution of microchannel flow passages: Thermohydraulic performance and fabrication technology", *Proceedings of the ASME international mechanical engineering congress exposition*, New Orleans, USA.

4) Kandlikar, S.G., Steinke, M.E., 2006, " Single phase liquid heat transfer in plain and enhanced microchannels", *Proceedings of ICNMM2006*, Limerick, Ireland.

5) Tesla, N., 1920, "Valvular conduit", U.S. Patent No. 1,329,559.

6) Chen,Yu-Tang, Kang,Shung-Wen, Wu,Lung-Chi, Lee,Sheng-Hua, 2008,"Fabrication and investigation of PDMS micro-diffuser/nozzle", *Journal of materials processing technology*, **198**, pp. 478-484.

7) Al-Faqheri,Wisam, Ibrahim,Fatimah, Thio,Tzer Hwai Gilbert, Aeinehvand, Mohammad Mahdi, Arof,Hamzah, Madou,Marc, 2015,"Development of novel passive check valves for the microfluidic CD platform", *Sensors and Actuators A:Physical*, **222**, pp. 245-254.

8) Pan,Tingrui, McDonald, J Scott, Kai, M Eleanor, Ziaie, Babak, 2005,"A magnetically driven PDMS micropump with ball check-vavles", *Journal of micromechanics and microengineering*, **15**, pp. 1021-1026.

9) Forster, F. K., Bardell, R. L., Afromowitz, M. A., Sharma, N. R., Blanchard, A., 1995, "Design, fabrication and testing of fixed-valve micro-pumps," *Proceedings of the ASME Fluids Engineering Division*, San Francisco, CA, U.S.A., **234**, pp. 39-44.

10) Bardell, R. L, 2000, "The diodicity mechanism of Tesla-type no-moving-parts valves,'' Ph. D. Dissertation, University of Washington, United States – Washington. Retrieved March 13, 2010, from Dissertations and Theses: A&I. (Publication No. AAT 0801983).

11) Paul, F. W., 1969, "Fluid mechanics of the momentum flueric diode," *IFAC Symposium on Fluidics,* Paper A1, Royal Aeronautical Society, pp. 1-15.

12) Truong, T. Q., Nguyen, N. T., 2003, "Simulation and optimization of Tesla valves,", *2003 Nanotech - Nanotechnology Conference and Trade Show*, San Francisco, CA, U.S.A., **1**, pp. 178-181.

13) Zhang, S., Winoto, S. H., Low, H. T., 2007, "Performance simulations of Tesla microfluidic valves," *Proceedings of the International Conference on Integration and Commercialization of Micro and Nanosystems*, Sanya, Hainan, China, Paper No. MNC2007-21107, **A**, pp. 15-19.

14) Gamboa, A. R., Morris, C. J., Forster, F. K., 2005, "Improvements in fixed-valve micropump performance through shape optimization of valves," *ASME Journal of Fluids Engineering*, **127** (2), pp. 339–346.

15) Thompson S.M, Walters D.K., Paudel B.J., Jamal, T., 2013, "Transitional and turbulent flow modeling in a Tesla valve", Proceedings ASME 2013 International Mechanical Engineering Congress & Exposition, California, USA.

16) Reed, J. L., 1993, "Fluidic rectifier", U.S. Patent No. 5,265,636.

17) S.M. Thompson, B.J. Paudel, T. Jamal, D.K. Walters, 2014,"Numerical investigation of multistaged Tesla valves", *ASME Journal of Fluids Engineering*, **136** (8).

18) Mohammadzadeh, K., Kolahdouz, E.M., Shirani, E., Shafii, M.B., 2012, "Numerical Investigation on the Effect of the Size and Number of Stages on the Tesla Microvalve Efficiency," Journal of Mechanics, 29 (3), pp. 527-534.

19) A. Bar-Cohen, J.J. Maurer, J.G. Felbinger, DARPA's Intra/Interchip Enhanced Cooling (ICECool) Program, in: CS MANTECH Conf., New Orleans, U.S.A., 2013: pp. 171–174.

20) T. Dixit, I. Ghosh, Review of micro- and mini-channel heat sinks and heat exchangers for single phase fluids, Renew. Sustain. Energy Rev. 41 (2015) 1298–1311.

21) Hsiao K., Wu C., Huang Y., 2014, "Fluid mixing in a microchannel with longitudinal vortex generators", *Chemical Engineering Journal*, **235**, pp. 27-36.

22) Karale, C. M., Bhagwat, S. S., Ranade V. V., 2013, "Flow and heat transfer in serpentine channels", *AIChE J.*, **59**, pp. 1814–1827.

23) A. Lee, G.H. Yeoh, V. Timchenko, J.A. Reizes, 2012, "Heat transfer enhancement in micro-channel with multiple synthetic jets", *Applied Thermal Engineering*, **48**, pp. 275-288.

24) Wang Y., Houshmand F., Elcock D., Peles Y., 2013, "Convective heat transfer and mixing enhancement in a microchannel with a pillar", *International Journal of Heat and Mass Transfer*, **62**, pp. 553-561.

25) Sui,Y., Lee, P.S., Teo, C.J., 2011,"An experimental study of flow friction and heat transfer in wavy microchannels with rectangular cross section", *International Journal of Thermal Sciences*, **50**, pp. 2473-2482.

26) Yonghui Xie, Jibing Lan, Di Zhang, 2012,"Flow and heat transfer in microchannels with Dimples and protrusions", *ASME Journal of Fluids Engineering*, **134** (2)

27) Zhizhao Che, Teck Neng Wong, Nam-Trung Nguyen, 2011,"Heat transfer enhancement by recirculating flow within liquid plugs in microchannels", *Elsevier International Journal of Heat and Mass Transfer*, **55**,pp. 1947-1956.

28) Saman Ebrahimi, Amin Hasanzadeh-Barforoushi, Amir Nejat, Farshad Kowsary 2014,"Numerical study of mixing and heat transfer in mixed electroosmotic/pressure driven flow through T-shaped microchannels", *Elsevier International Journal of Heat and Mass Transfer*, **75**,pp. 565-580.

29) Yoav Peles, Yingying Wang, 2014,"An experimental study of passive and active heat transfer enhancement in microchannels", *ASME Journal of Heat Transfer*, **136**(3).

30) Gian Luca Morini, Yahui Yang, 2013,"Guidelines for the determination of single-phase forced convection coefficients in microchannels", *ASME Journal of Heat Transfer*, **135**(10).

31) Thompson, S. M., Ma, H. B., Wilson, C. A., 2011, "Investigation of a flat-plate oscillating heat pipe with Tesla-type check valves," *Experimental Thermal and Fluid Science,* **35** (7), pp. 1265-1273.

32) Kays, W.M., and M.E. Crawford, Convective Heat and Mass Transfer, 3rd ed. McGraw-Hill, New York, 1993.

33) Fiebig, M., 1998,"Vortices, generators and heat transfer", *Trans IChemE*, **76**, pp.108-123.

APPENDIX A

DESIGN CORRELATIONS FOR TESLA VALVE

Design correlation derived for Tesla valves are listed below.

Friction coefficient correlations

	Forward flow	Reverse flow
First valve	$\bar{f}_{1,\text{fwd}} \cong 0.180742(\text{Re}^{0.876})$	$\bar{f}_{1,\text{rev}} \cong 0.0912696(\text{Re}^{0.663})$
Last valve	$\bar{f}_{\infty,\text{fwd}} \cong 0.156781(\text{Re}^{0.828})$	$\bar{f}_{\infty,\text{rev}} \cong 0.0863161(\text{Re}^{0.649})$

Pressure diodicity correlations

First valve	Last valve
$Di_P \cong 0.975 + 0.000435(\text{Re}^{1.422})$	$Di_P \cong 0.958 + 0.000574(\text{Re}^{1.312})$

Nusselt number correlations

	Forward flow	Reverse flow
First valve	$\overline{\text{Nu}}_{1,\text{fwd}} \cong 0.126\text{Re}^{0.276}\text{Pr}^{1/3}$	$\overline{\text{Nu}}_{1,\text{rev}} \cong 0.056\text{Re}^{0.789}\text{Pr}^{1/3}$
Last valve	$\overline{\text{Nu}}_{\infty,\text{fwd}} \cong 0.167\text{Re}^{0.361}\text{Pr}^{1/3}$	$\overline{\text{Nu}}_{\infty,\text{fwd}} \cong 0.087\text{Re}^{0.699}\text{Pr}^{1/3}$

Thermal diodicity correlations

First valve	Last valve
$Di_\text{T} \cong 0.59 + 0.072(\text{Re}^{0.69})$	$Di_\text{T} \cong 0.54(\text{Re}^{0.33})$